Chemical Science

ROYAL SOCIETY OF CHEMISTRY

REVIEW

View Article Online
View Journal

Cite this: DOI: 10.1039/d6sc00853d

Anode-free solid-state sodium batteries: navigating the challenges toward high energy density

Yi-An Zhao,[a] Ge Sun,[b] Heng Jiang,*[a] Zhixuan Wei*[a] and Fei Du*[a]

Anode-free solid-state sodium batteries (AFSSBs) represent a transformative paradigm, positioning themselves as the ultimate avenue to unlock the high-energy-density potential of sodium-based electrochemistry. However, their practical implementation is hindered by fundamental challenges, including inadequate solid electrolyte properties, unstable interfacial contacts, and uncontrolled sodium deposition morphology. This review provides a timely and systematic analysis of this evolving frontier. Following a clear presentation of the existing challenges, we organize and discuss emerging strategies spanning three key areas: the development of novel electrolytes, the construction of stable interfaces, and the optimization of current collector substrates. The pivotal role of advanced characterization in elucidating underlying mechanisms is also underscored. In the final section, we outline a forward-looking roadmap, identifying critical research pathways to accelerate the translation of AFSSB technology from promising prototypes toward practical, next-generation energy storage solutions.

Received 31st January 2026
Accepted 18th March 2026

DOI: 10.1039/d6sc00853d

rsc.li/chemical-science

1. Introduction

The quest for efficient electrical energy storage has been a defining challenge of modern society.[1,2] While lithium-ion batteries (LIBs) have undeniably powered the portable electronics revolution and are now propelling the electric vehicle transition, their long-term sustainability faces fundamental questions regarding the geopolitical constraints and resource scarcity of lithium and cobalt.[3–5] Within this context, sodium–ion battery (SIB) technology, once a contemporary of early LIB research in the 1970s–80s, has experienced a profound renaissance over the past decade.[6,7] Initially sidelined due to the superior energy density achieved by LIBs, SIBs operated by the same "rocking-chair" mechanism have re-emerged extensively, highlighting a compelling economic and strategic imperative: the critical need for abundant, globally distributed, and low-cost materials for grid-scale storage and mass-market electrification.[8–11]

This renewed investment has driven rapid progress in SIB materials chemistry as well. A diverse portfolio of cathode materials has been developed, primarily falling into three categories: layered transition metal oxides, polyanionic compounds (*e.g.*, $Na_3V_2(PO_4)_3$, $Na_4Fe_3(PO_4)_2P_2O_7$), and Prussian blue analogues.[12–18] Paired with inexpensive, hard-carbon-based anodes, these systems have enabled the first wave of SIB commercialization by CATL, TIAMAT and Natron Energy, *etc.*[19,20] Contemporary SIBs now deliver energy densities in the range of 120–160 W h kg^{-1}, achieving parity with the well-established lithium iron phosphate (LFP) chemistry.[20–24] Paradoxically, this success highlights the core dilemma of the current SIB technology: the energy density of conventional "rocking-chair" SIBs is approaching a practical ceiling imposed by the specific capacities and operating voltages of its constituent materials.[9,23,25] This can be primarily attributed to the much larger size and weight of sodium ions compared to lithium counterpart. Consequently, they struggle to compete with higher-energy nickel-rich LIBs for premium applications.[25] On the other hand, their overarching economic advantage is being challenged.[26] The recent significant decline in lithium carbonate prices has dramatically reduced LFP battery costs, squeezing the projected economic margin for SIBs and forcing a strategic re-evaluation.[27]

Based on the above discussion, the future of SIBs lies not in head-to-head competition across all fronts with LIB technologies but in strategic complementation.[28] Its most promising applications are in domains where cost, safety, and sustainability outweigh the need for maximum energy density, such as large-scale stationary energy storage, low-speed electric vehicles, and as a high-performance replacement for lead-acid batteries.[28–32] As an inspiring example, the HiNa company has established GWh-scale battery cell production line for SIBs, making it a worldwide pioneer in achieving commercial applications of sodium-ion battery technology in both hundred-megawatt-hour level energy storage power stations and the commercial vehicle sector.[24] Their newly operational capacity of New Energy Storage Power Station Technology stands at 50 MW/100 MW h.[33] Nevertheless, to secure these markets decisively

[a]*Key Laboratory of Physics and Technology for Advanced Batteries (Ministry of Education), State Key Laboratory of High Pressure and Superhard Materials, College of Physics, Jilin University, 130012 Changchun, China. E-mail: jiangheng@jlu.edu.cn; zhixuanwei@jlu.edu.cn; dufei@jlu.edu.cn*

[b]*Jovision Energy Technology Co., Ltd., 230031 Hefei, China*

with the expanding demand for green energy, SIBs must not only preserve a clear cost advantage but also push beyond the LFP energy density benchmark. This requires a fundamental architectural innovation, moving beyond mere material optimization.[34,35]

As a revolutionary solution to the aforementioned issues, the integration of the anode-free configuration with solid-state electrolytes represents the most promising, albeit challenging, path to this goal.[36,37] The anode-free (or strictly speeking, initial anode-free) design eliminates the pre-stored active host material (*e.g.*, hard carbon, sodium metal), plating metallic sodium from cathode desodiation directly onto the current collector during charge.[38–41] As illustrated in Scheme 1a, this maximizes the energy density by utilizing the cell's mass almost entirely for the sodium source (cathode) and removing the weight and volume of a permanent anode.[42–44] This configuration also offers intrinsic cost advantages. specifically, the eliminated anode host material simplifies manufacturing and reduces material costs, while the use of aluminum (rather than copper) as the current collector in sodium systems also provides substantial savings over lithium-ion counterparts. To this end, efforts have been devoted to developing anode-free cells based on liquid electrolytes. However, numerous challenges emerge, especially rampant dendrite growth and poor coulombic efficiency derived from uncontrolled and uneven metal deposition on current collector.[44] Solid-state electrolytes (SSEs) offer a potential

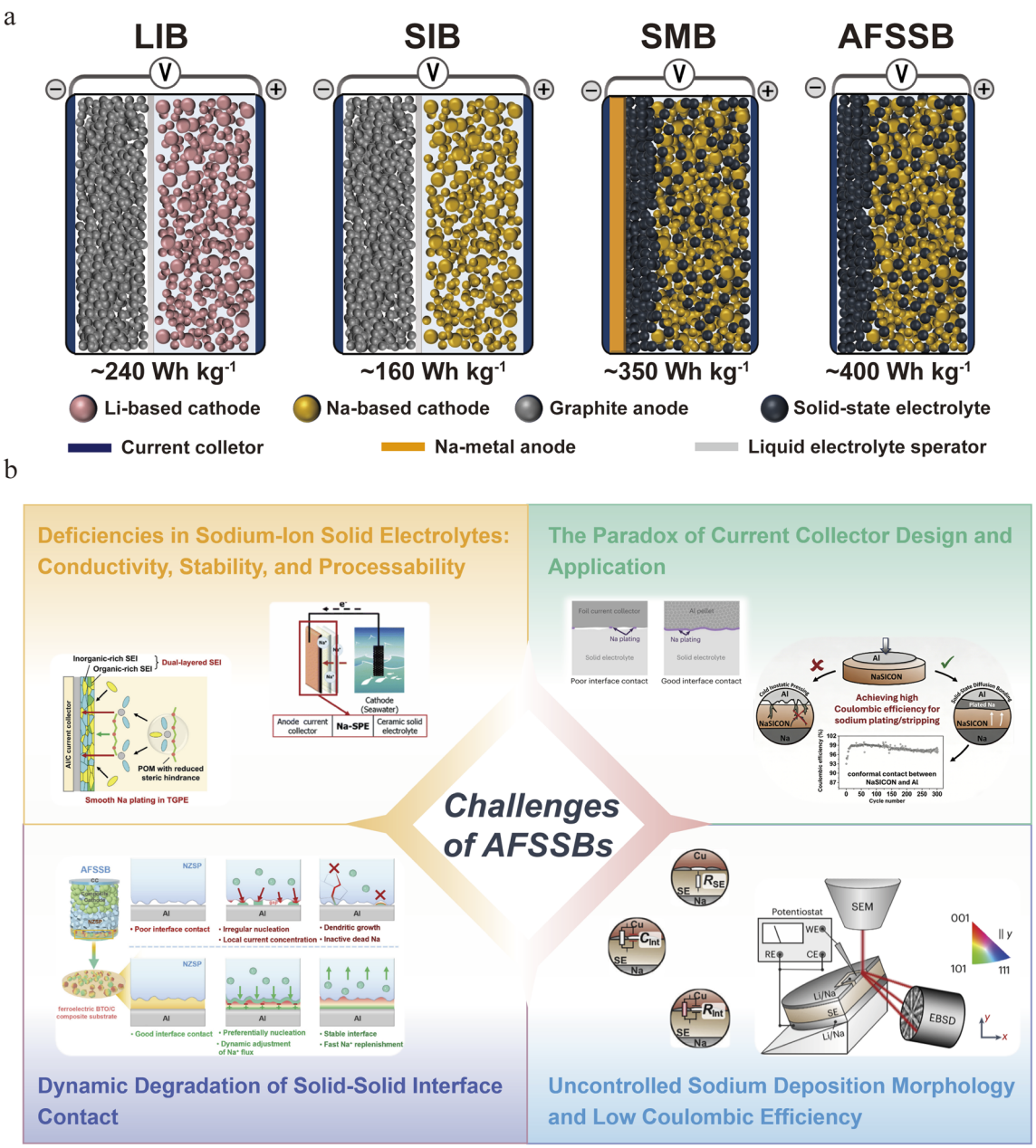

Scheme 1 (a) Illustration of configuration and comparison of cell performance for LIB, SIB, SMB, and AFSSB systems;[5,43,49–52] (b) key challenges of state-of-art AFSSBs.

solution, with their high mechanical strength to physically block dendrites and superior (electro)chemical stability.[36,46,47] Therefore, the anode-free solid-state sodium metal battery is increasingly viewed not merely as an incremental step, but as a potential endgame for high-energy-density SIBs, promising to unlock the full theoretical potential of sodium chemistry by addressing its most fundamental stability and safety challenges.[1,45,48]

Given the nascent stage of this promising technology, this report aims to systematically review the current progress in anode-free solid-state sodium metal battery. We first elucidate the fundamental challenges spanning from materials to interfaces, then evaluate corresponding innovative solutions across electrolyte design, interface engineering, and current collector optimization. We also highlight the critical role of advanced characterization in guiding rational design. Finally, the article concludes with a forward-looking perspective on key research priorities. We intend for this analysis to stimulate focused efforts and cross-disciplinary collaboration towards overcoming the remaining barriers.

2. Challenges in anode free solid state sodium metal batteries

The practical realization of (initial) anode-free solid-state sodium battery (AFSSB) configuration is hindered by a integration of interconnected scientific and engineering challenges that covers both bulk material properties and atomic-scale interfacial phenomena. These issues collectively degrade coulombic efficiency, accelerate capacity fade, and pose significant safety risks, forming a significant barrier to commercialization advances. The core challenges can be delineated into the following critical aspects.

2.1 Deficiencies in sodium-ion solid electrolytes: conductivity, stability, and processability

The foundation of any solid-state battery is its electrolyte to transfer charge carriers between electrodes.[53] For AFSSBs, the ideal solid-state electrolyte (SSE) must simultaneously satisfy a set of requirements that are often unfortunately conflicting. First, while several sodium superionic conductors (NASICON-type, sulfides) have achieved decent bulk ionic conductivities ($>10^{-3}$ S cm^{-1} at room temperature), they still fall behind their liquid counterparts and the best lithium SSEs.[54] Furthermore, in practical applications, they continue to face critical challenges such as poor electrode/electrolyte interfacial compatibility and high grain-boundary resistance.[55] This intrinsic transport limitation increases cell impedance and polarization, exacerbating inhomogeneous sodium deposition at high current densities. More critically, the thermodynamic instability of most SSEs (especially sulfides and several oxides) against metallic sodium is a fundamental issue. This leads to the spontaneous formation of a passivating interphase – a solid electrolyte interphase (SEI) at the anode side.[56] Unlike the dynamically stable SEI in liquid systems, this interphase in solid-state systems is often highly resistive, brittle, and continues to grow, consuming both the electrolyte and active sodium.[57,58] Furthermore, the mechanical properties and processability of SSEs are paramount. They must be sufficiently ductile or formable to maintain intimate contact under stack pressure, yet robust enough to resist sodium dendrite penetration.[59] The development of a sodium SSE that optimally balances high ionic conductivity, (electro)chemical stability, mechanical resilience, and scalable thin-film fabrication remains a primary material-level challenge.

2.2 The paradox of current collector design and application

In an anode-free cell, the role of the current collector transforms from a mere electron conductor to a component that critically determines the kinetics of sodium nucleation and growth. Currently, there are no established design principles for this critical component. Its surface chemistry, morphology, crystallographic orientation, and electronic properties profoundly influence the nucleation overpotential, the density of nucleation sites, and the subsequent growth morphology of sodium.[43] A heterogeneous surface often leads to spatially irregular nucleation, resulting in isolated, large islands rather than a smooth, uniform film.[60,61] The role of surface coatings (*e.g.*, sodiophilic interlayers like Sn, Sb, or carbon) is being explored, but their long-term stability, impact on energy density, and interaction with the SSE during repeated cycling are poorly understood. The fundamental question of how to engineer a current collector that promotes low-barrier, homogeneous nucleation and guides laterally uniform, dense sodium plating is wide open.

2.3 Dynamic degradation of solid–solid interface contact

The anode|SSE interface is a rigid, solid–solid junction that lacks the dynamic adaptability of liquid electrolytes, which can flow to accommodate volume changes.[62,63] This contact is highly sensitive to volume changes and morphological evolution during cycling. Specifically, sodium plating expands the interface, while stripping contracts it, creating repetitive mechanical stress. This process can lead to interfacial delamination, void formation, and eventually loss of contact.[64] Voids are particularly detrimental as they create localized current hotspots, guiding subsequent sodium deposition to the remaining contact areas and accelerating uneven growth. In a nutshell, poor solid–solid interfacial contact leads to high interfacial resistance and uncontrolled sodium dendrite growth.[65] In other words, maintaining spatially uniform interfacial contact under dynamic plating/stripping is a critical mechanical challenge.[66] It requires careful optimization of stack pressure, SSE viscoelastic properties, and the design of compliant or adaptive interfacial layers.

2.4 Uncontrolled sodium deposition morphology and low coulombic efficiency

The ultimate manifestation of the aforementioned problems is the uncontrolled, inhomogeneous deposition of sodium metal. Driven by uneven ion flux, heterogeneous nucleation, and interfacial instability, sodium tends to deposit in fractal, mossy,

or dendritic morphologies. This porous structure increases the electrolyte|Na contact area, accelerating side reactions and trapping isolated, "dead" sodium. The repeated breaking and reforming of the SEI on this evolving surface leads to continuous consumption of sodium and electrolyte, which is reflected in low and decaying coulombic efficiency.[62,63,66] This inefficiency is catastrophic in an anode-free cell with zero excess sodium, as every lost coulomb directly depletes the limited reservoir in the cathode, leading to rapid capacity decay. Furthermore, dendrites that penetrate the SSE can cause internal short circuits. Understanding the dynamic, non-equilibrium processes that govern sodium nucleation and growth within the constrained geometry of a solid-state system is a central challenge. This fundamental challenge necessitates the application of advanced, non-destructive *in situ* characterization techniques to visualize sodium plating behavior. Although some studies have utilized advanced characterization techniques to investigate solid-state electrolytes, the buried, solid-state nature of the key interfaces creates a major obstacle for such observation, leaving a critical gap in mechanistic understanding.[67–71]

In summary, the challenges of practical AFSSBs are cascade of interdependent challenges rooted in the fundamental mismatch between the dynamic process of metal electrodeposition and the static nature of solid-state components, as outlined in Scheme 1b. Crucially, these issues are not isolated, but rather form a detrimental, self-reinforcing cycle where interfacial degradation promotes inhomogeneous plating, which in turn accelerates further degradation. The eventual breakthrough demands not just improvements in individual components, but a holistic, co-design strategy that simultaneously addresses ionic transport, interfacial chemistry, and mechanical integrity across the entire cell architecture.

3. Current strategies for anode-free solid-state sodium metal batteries

As mentioned, addressing the multifaceted challenges outlined in Section 2 requires a holistic and integrated approach. Recent research has converged on several strategic directions that directly target these interconnected issues: electrolyte innovations to overcome the conductivity-stability trade-off (Section 3.1), current collector engineering to establish rational design principles (Section 3.2), interface modification to improve the solid–solid contact (Section 3.3), and advanced characterization to unravel the mysteries of sodium deposition (Section 3.4), which are discussed in detail in the following section.

3.1 Electrolyte engineering: balancing conductivity, stability, and processability

To overcome the deficiencies of conventional solid electrolytes, researchers are developing novel composite systems that decouple ionic transport from interfacial reactivity. A pioneering strategy to circumvent the intrinsic conductivity/stability trade-offs in single-phase SSEs is the design of hybrid systems. For instance, Zhou's group proposed a "liquid-in-solid" electrolyte, where a liquid ether electrolyte (1 M $NaPF_6$-diglyme/G2 electrolytes) known for its superior interfacial stability with Na metal is confined within the nanopores of a rigid, Na^+-conductive zeolite framework (Na-SSZE).[72] Such a "liquid-in-solid" electrolyte represents a promising strategy, as

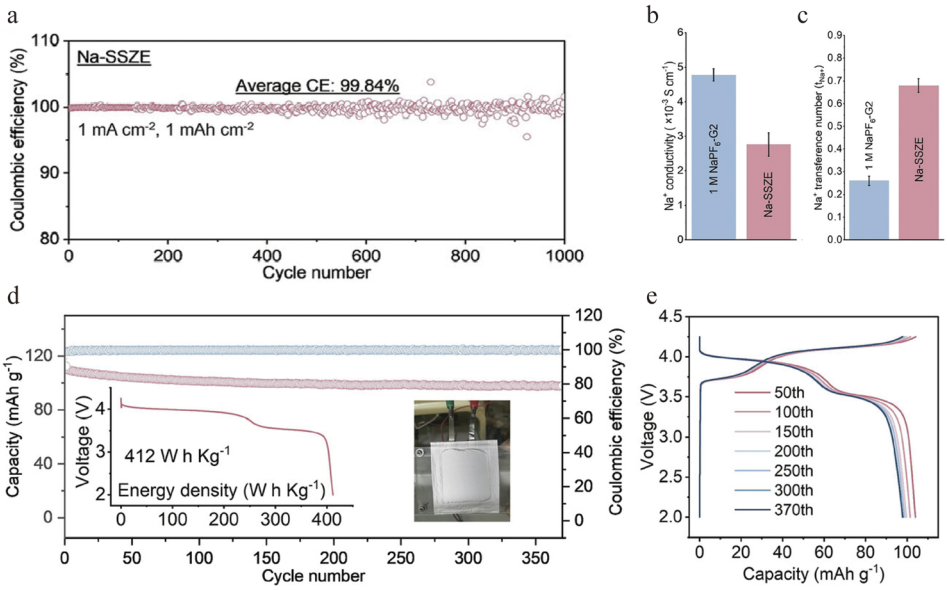

Fig. 1 Implementing a "liquid-in-solid" design to concurrently achieve high ionic conductivity and interfacial reversibility in solid-state sodium batteries. (a) Plating-stripping CEs of Na||Al batteries using the Na-SSZE. (b and c) Ion conductivity (b), and transference number (c) of ether electrolytes and Na-SSZE. (d) Cycling stability of high-voltage anode-free pouch cells using the Na-SSZE. The inset shows the galvanostatic discharge curves *versus* the gravimetric energy density in pouch cells (tested at current density of 0.49 mA cm^{-2}, without extra pressure). (e) Selected charge–discharge curves of anode-free cells using the Na-SSZE. Copyright 2024, Wiley-VCH GmbH.

it is capable of delivering the demanding coulombic efficiency (CE) required for Na plating/stripping while also resisting oxidative decomposition at high voltages, which is crucial for building stable anode-free Na batteries. By integrating the high-voltage stability of a silica-aluminum oxide zeolite with the ultra-high Na plating/stripping capability of an ether electrolyte, the "liquid-in-solid" Na-SSZE design delivers excellent stability and a 99.84% CE (Fig. 1a). Through a dual-mode ion transport mechanism, the system achieves an ionic conductivity of 2.76×10^{-3} S cm^{-1} and a Na^+ transference number of 0.68 at 20 °C (Fig. 1b and c). With the application of the proposed electrolyte, the assembled anode-free pouch cell delivers an energy density of 412 W h kg^{-1} (based on the active material of both cathodes and anodes), and retains 89.2% capacity after 370 cycles (Fig. 1d and e), showing competitiveness against common commercial graphite||NCM811 Li-ion batteries in terms of energy density and cost. This work establishes the "liquid-in-solid" configuration as a viable design paradigm for integrating interfacial reversibility and bulk stability in AFSSBs.

Wang's group developed a polymer-based strategy that addresses Na^+ solvation and the SEI structure, and enhances safety, to achieve long-cycle-life quasi-solid-state AFSSBs.[57] They engineered a gel polymer electrolyte from polyoxymethylene (POM) (Fig. 2a), forming an anion-rich Na^+ solvation structure with weak solvation ability. This anion-rich solvation structure reduces the Na^+ desolvation energy barrier, thereby enhancing the Na^+ transference number and accelerating interfacial charge transfer. Consequently, the quasi-solid-state electrolyte exhibits high ionic conductivity (Fig. 2b) and promotes the formation of a robust, bilayer SEI that is composed of a NaF-rich, electron-blocking inner layer and a flexible organic outer layer, and thus enables highly reversible Na plating/stripping with an average coulombic efficiency of 99.75% (Fig. 2c). Full AFSSB cells with a commercial NVP cathode deliver a long cycle life of 500 cycles with 79% capacity retention at 1C (Fig. 2d). The 1.2 Ah pouch cells retain over 81% capacity after 200 cycles (Fig. 2e), achieving high specific energies of 352 W h kg^{-1} based on active mass and 190 W h kg^{-1} at the cell level. Compared to conventional Na-ion cells using an NVP cathode and hard carbon anode, the quasi-solid-state anode-free configuration shows a 36.6% improvement in gravimetric energy density and a 49% enhancement in volumetric energy density (Fig. 2f). Furthermore, they demonstrate excellent safety, with no failure or thermal runaway observed upon nail penetration in ambient air (Fig. 2g).

Interestingly, Passerini's group recently reported an anode-free sodium-seawater battery (Na-SWB), a configuration that differs fundamentally from conventional rechargeable cells.[73] The cell employs an anode-less configuration, wherein the anode compartment comprises solely a current collector (Cu foil) and a solid-polymer electrolyte (Na-SPE). This compartment is physically separated from the cathode by a NASICON solid-electrolyte layer, with carbon fabric serving as the cathode current collector. The cross-linked solid polymer electrolyte is composed of PEO, NaFSI, and $Pyr_{14}FSI$ ionic liquid in a 10 : 1 : 4 molar ratio (denoted as 10(PEO)-NaFSI-4($Pyr_{14}FSI$)) and exhibits an ionic conductivity of 1.43 mS cm^{-1} at 20 °C (Fig. 3a). This "anode-free" setup enables reversible deposition and stripping of sodium metal directly on the current collector during cycling, realizing a closed "power-to-metal" and "metal-to-power" energy cycle (Fig. 3b and c). To stabilize such an anode-free operation, a highly conductive and mechanically compliant solid-polymer electrolyte is essential. Its soft, adaptive nature helps maintain interfacial contact during sodium plating/stripping, mitigating issues like pore formation and dendrite growth. In this anode-free full cell, the system delivered a high round-trip energy efficiency of 94.1% and stable operation over 25 cycles (Fig. 3d). Furthermore, the system functions as an efficient sodium harvesting platform, electroplating a dense sodium metal layer approximately 50 μm thick on an aluminum current collector (Fig. 3e and f). Beyond demonstrating the promise of seawater based systems for large scale stationary storage, this work provides a versatile platform for research into next generation sodium battery technologies.

Apart from electrolyte design, Wuliang Feng *et al.* demonstrated that trace LiN_3 additive into hybrid solid-state gel electrolyte (composed of a polyoxyethylene (PEO) matrix with a 1 M $NaPF_6$ in diglyme liquid phase (15 wt% liquid content) can concurrently establish electrostatic shielding and a highly ion–conductive interface, effectively suppressing sodium dendrite growth in anode-free quasi solid-state sodium batteries.[74] COMSOL simulations revealed that Li^+ addition raised the electrolyte's relative permittivity by two orders of magnitude, significantly homogenizing electric field and charge density distributions (Fig. 4a). *In situ* optical microscopy corroborated this, showing smooth, dendrite-free sodium deposition in the LiN_3-modified electrolyte (Fig. 4b). TEM and XPS analyses further indicated that LiN_3 decomposition formed an ultrathin (3–4 nm) interfacial phase with a Na_3N-rich lattice, which combines high ionic conductivity with high mechanical strength (Fig. 4c). As a result, symmetric cells achieved a high critical current density of 22.0 mA cm^{-2} (Fig. 4d), while anode-free full cells retained 81.6% capacity after 400 cycles at 0.5C and delivered an energy density of 256.8 Wh kg^{-1} (based on the total weight of electrode and electrolyte) (Fig. 4e and f). This work offers a precise electrolyte-design strategy for interfacial control, providing a viable route toward high-energy-density, long-life sodium metal batteries.

3.2 Current collector design: engineering the nucleation substrate

Recognizing the current collector's critical role, new design principles are emerging to govern sodium nucleation and initial growth. Meng's group established four key design principles for realizing anode-free solid-state sodium metal batteries: (i) an electrochemically stable electrolyte; (ii) intimate interfacial contact; (iii) a dense solid electrolyte; (iv) a dense current collector. Following these principles, $Na_4B_{10}H_{10}B_{12}H_{12}$ (NBH) (Fig. 5a), which exhibits electrochemical stability against sodium metal, was selected as the solid electrolyte.[43] This choice effectively mitigated sodium inventory loss, raising the initial coulombic efficiency (ICE) of a half-cell from 4% with an unstable Na_3PS_4 electrolyte to 64% (Fig. 5b). Subsequently, they

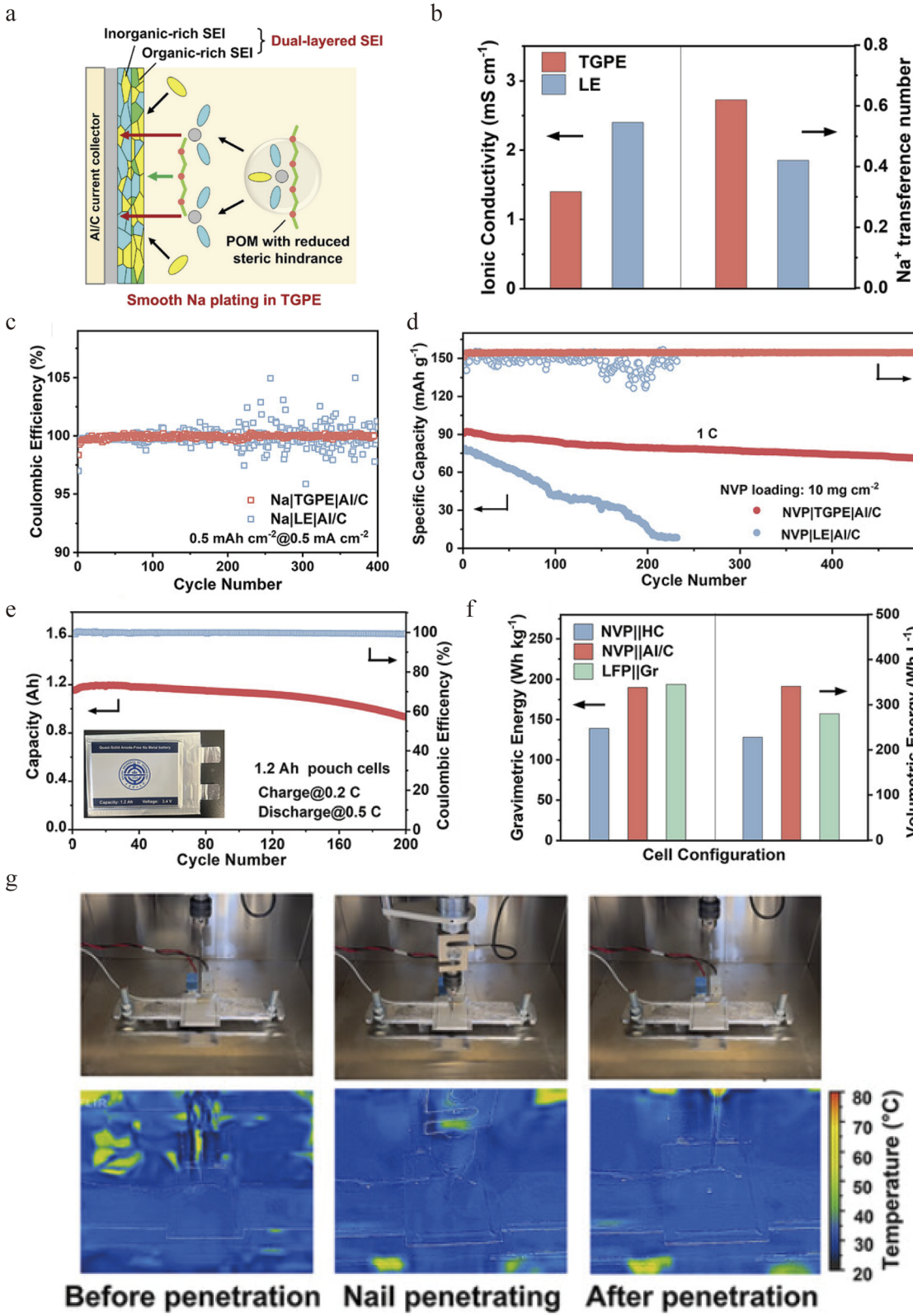

Fig. 2 Achieving high safety and energy density with a quasi-solid-state, anion-rich gel polymer electrolyte. (a) Schematic illustration of utilizing polymer with reduced local steric hindrance and Na^+ solvation to direct the formation of weakly solvating polymer-stabilized anion-rich Na^+ solvation structure and inorganic–organic dual-layered interphase for smooth Na metal deposition. (b) A comparison of TGPE and LE in ionic conductivity and Na^+ transference number. (c) CE of Na|TGPE|Al/C and Na|LE|Al/C asymmetric cells with a capacity of 0.5 mA h cm^{-2} at 0.5 mA cm^{-2}. (d) Long-term cycling stability at 1C for 500 cycles for NVP|TGPE|Al/C and NVP|LE|Al/C cells. (e) Cycling capability and CE of 1.2 Ah quasi-solid-state anode-free pouch cells. (f) A comparison in gravimetric and volumetric energy of quasi-solid-state pouch cells based on NVP||Al/C, NVP||HC and LPF||Gr configurations. (g) Infrared thermography of a quasi-solid-state anode-free pouch cell in a fully charged state upon nail penetration. Copyright 2025, Wiley-VCH GmbH.

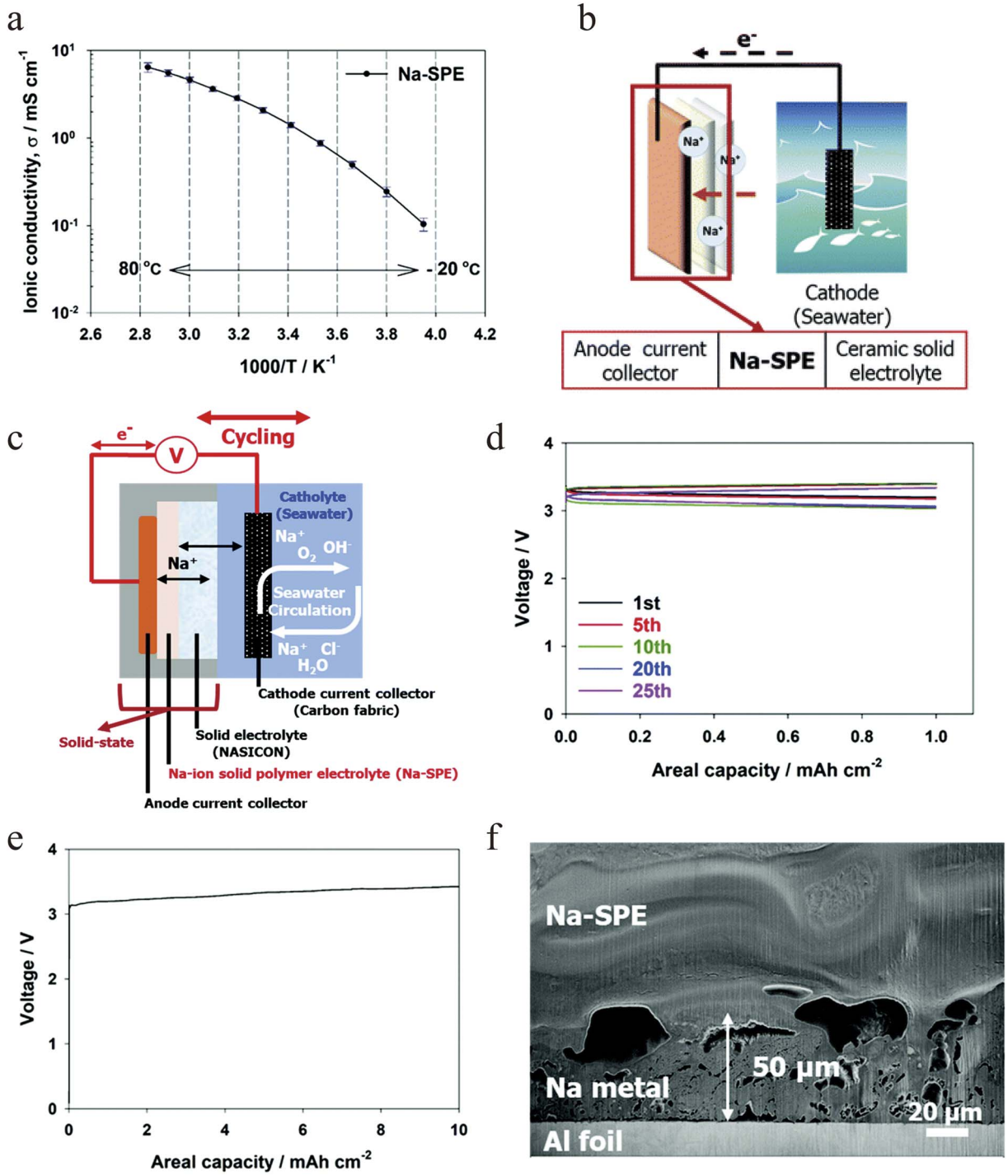

Fig. 3 Enabling reversible sodium deposition in anode-free seawater batteries with a solid polymer electrolyte. (a) Ionic conductivity of the Na-SPE. (b) Schematic illustration of the anode-less Na-SWBs (c) schematic illustration of the cell setup for a Na–seawater battery (Na-SWB) employing the Na-SPE. (d) Charge/dis-profiles of galvanostatic cycle, applying a current density of 0.1 mA cm^{-2} $t = 20 \pm 3$ °C. (e) Charge voltage profile of a modified Na-SWB for sodium metal harvesting. (f) SEM-FIB image of the Na metal harvested anode. Copyright 2022, the Royal Society of Chemistry.

used an innovative cold-pressed aluminum-powder pellet to replace conventional aluminum foil as the current collector, which achieved uniform and intimate interfacial contact (Fig. 5c), promotes more complete stripping of sodium metal, enhancing its reversibility. Consequently, it increased the ICE to 93%, reduced the interfacial impedance (Fig. 5d–e), and substantially improved the critical current density from 1.2 mA cm^{-2} (with conventional Al foil) to 6.0 mA cm^{-2} (Fig. 5f–g). To investigate the impact of current collector porosity on the reversibility of sodium plating/stripping, the cells were

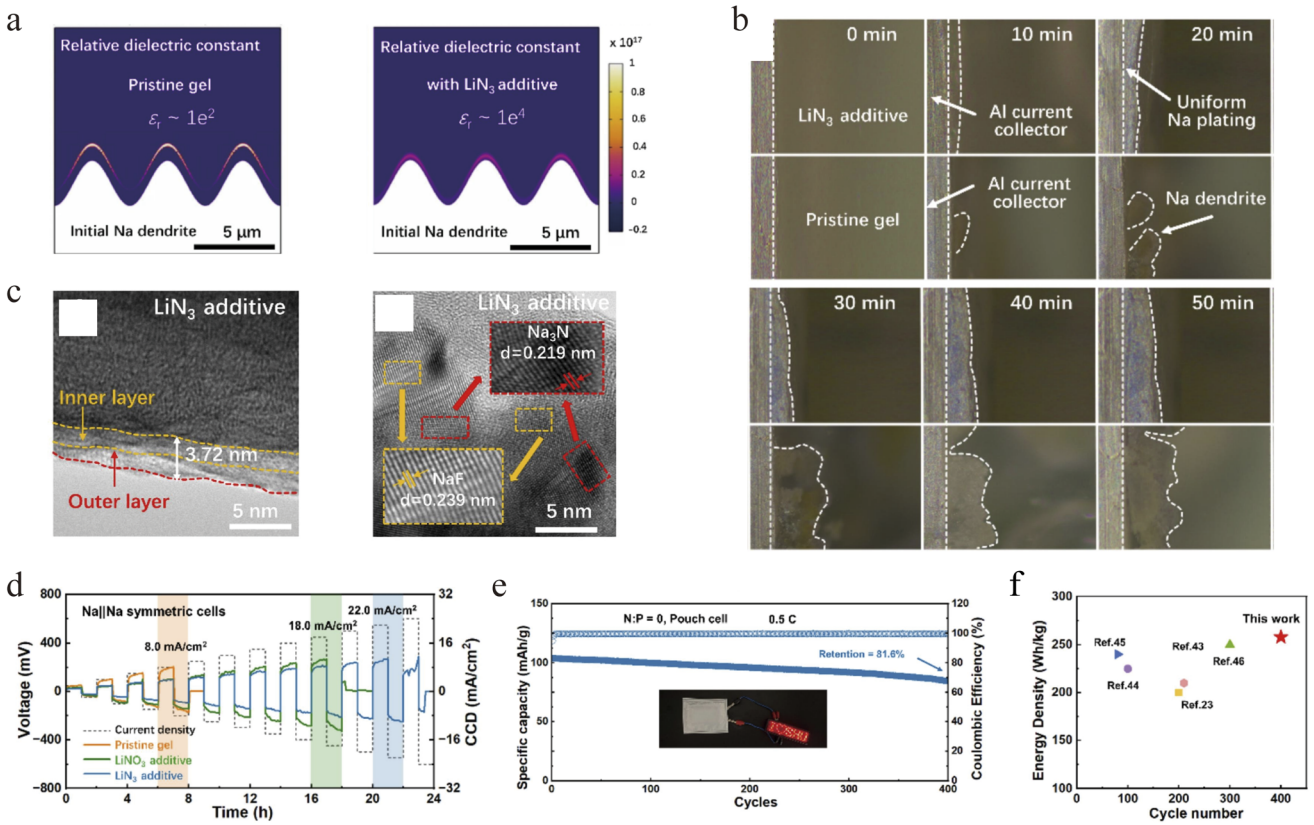

Fig. 4 Establishing electrostatic shielding and a conductive Na_3N-rich interface *via* LiN_3 to achieve high-CCD and stable cycling in anode-free sodium batteries. (a) Relative dielectric constant distribution in the pristine gel the gel with LiN_3 additive at an external electric field. (b) Optical microscope cross-sectional images of Na plating behavior in gel without and with LiN_3 additive. (c) TEM images of the interphase in the gel electrolyte with LiN_3 additive. (d) Critical current density of the Na symmetric cells. (e) Cycling of the pouch type AFSSBs with LiN_3 additives. (f) Energy density and cycling comparison to previously reported anode-free configurations. Copyright 2025, Elsevier B.V.

examined using FIB-SEM after one cycle. The results (Fig. 5h–j) show that during plating, sodium metal becomes trapped in pores present in the current collector. Because the solid-electrolyte separator cannot infiltrate these pores, sodium remaining inside them becomes ionically insulated after stripping at the solid electrolyte/current collector interface (Fig. 5k). Consequently, aluminum was identified as essential for achieving reversible plating/stripping, as its softness allows it to become highly dense after cold-pressing during cell assembly, thereby minimizing porosity. Based on this design, a full AFSSB cell with a $NaCrO_2$ cathode demonstrated remarkable performance at 40 °C under 10 MPa, cycling stably for 400 cycles with 70% capacity retention and an average CE as high as 99.96% (Fig. 5l and m). This work underscores that the current collector's morphology and microstructure are as critical as its chemistry, providing a blueprint for designing substrates that promote uniform sodium plating.

Surface decoration can be considered as another effective strategy to enhance the sodium plating kinetics onto current collector. Sakamoto's group addressed the current collector|SE interfacial challenge through a general alloy-based interface-engineering strategy.[61] Specifically, they introduced an ultra-thin gold coating (~96 nm) on an aluminum current collector in direct contact with a NASICON solid electrolyte, which significantly enhanced interfacial wettability thanks to the sodiophilic properties of Au. This modified Al current collector enabled reversible sodium deposition of 2.0 mA h cm^{-2} at 0.5 mA cm^{-2} with a low interfacial resistance of only ~7 Ω cm^2 (Fig. 6a and b). The plated sodium layer was dense and uniform, showing no obvious dendrite formation (Fig. 6c), while gold was found to diffuse uniformly throughout the sodium layer, confirming the guiding role of alloying in homogeneous nucleation. Although the initial coulombic efficiency was ~86.5% due to incomplete alloying during the first stripping (Fig. 6d), it stabilized at 94% after 10 cycles (Fig. 6e), indicating good electrochemical reversibility. This work presents an effective interface-regulation approach for AFSSBs by the facile surface treatment of current collectors, and underscores the need to develop low-cost, sodiophilic alloy materials.

Nazar's group employed solid state diffusion bonding to join an aluminum current collector (UV-ozone-treated) with a NaSICON solid electrolyte ($Na_{3.4}Zr_2Si_{2.4}P_{0.6}O_{12}$) under 620 °C and 50 MPa, physically forming a void free conformal contact interface (Fig. 7a).[75] This intimate interface effectively suppressed current focusing, enabling uniform sodium deposition exceeding 12.5 mA h cm^{-2} (~110 μm thick) at 0.5 mA cm^{-2} (Fig. 7b). In contrast, a cold isostatic pressed reference sample with a 1–2 μm interfacial gap exhibited early current

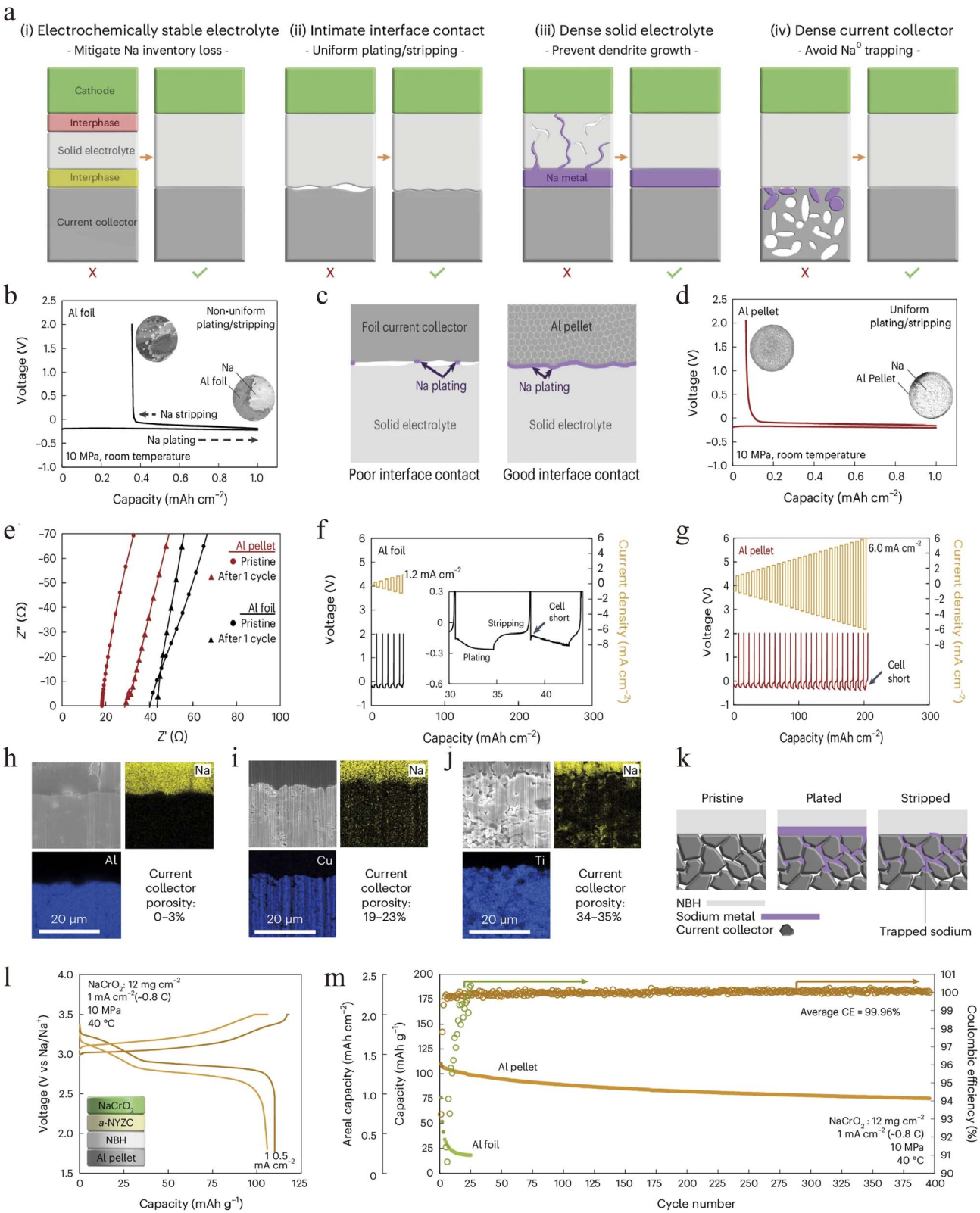

Fig. 5 Establishing four design principles for enabling anode-free sodium all-solid-state batteries. (a) Schematic illustrating the four requirements for enabling an anode-free all-solid-state battery. (b) Plating/stripping behavior at 1 mA cm^{-2} current density for Al foil. (c) Schematic illustrating the ability of aluminium powder to form intimate contact with the solid electrolyte layer (d) plating/stripping behavior at 1 mA cm^{-2} current density for al pellet current collectors. (e) Impedance measurements before and after cycling Al foil and Al pellet cells (tested at current density of 0.5 mA cm^{-2}, at 1.3 MPa pressure). (f and g) Critical current density when cycling 4 mA h cm^{-2} capacity with Al foil with inset showing fine details of the voltage profile during cell failure (f) and Al pellet current collectors (g). (h–j) FIB-SEM cross section views of Al (h), Cu (i) and Ti (j) current collectors after one plate/strip cycle with EDs mapping. (k) schematic of Na trapping mechanism for porous current collectors. (l and m) Voltage curves of a sodium anode-free solid-state full cell including a constant voltage hold at 3.5 V (l) and cell capacity over 400 cycles for the same cell combined with Al foil data for comparison (m). Copyright © 2024, the Author(s), under exclusive licence to Springer Nature Limited.

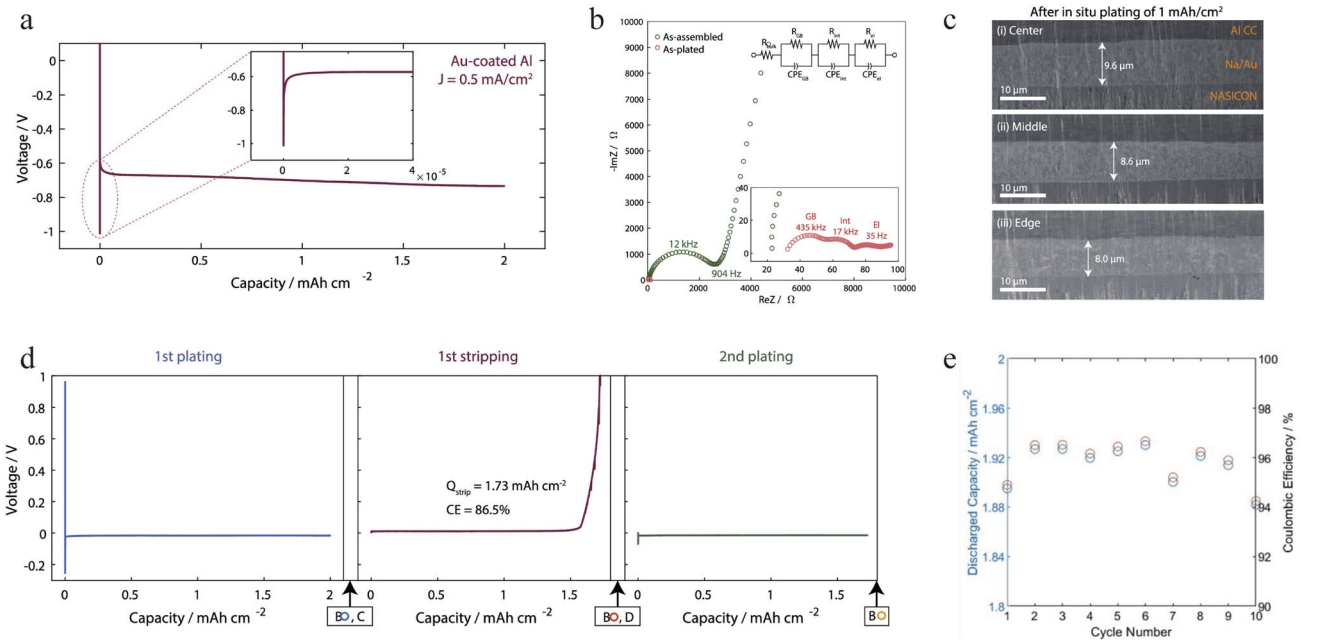

Fig. 6 Enabling uniform sodium deposition *via* a sodiophilic Au interlayer for anode-free solid-state sodium batteries. (a) *In situ* plating of Na using a AFSSB cell design. Voltage profiles of *in situ* Na plating on Au – Al foil at 0.5 mA cm^{-2}. (b) Impedance spectra before (green circles) and after (red circles) *in situ* plating of Na on a Au – Al cc. (c) Cross-sectional images of *in situ* Na anodes at various electrode positions: (i) center, (ii) middle, and (iii) edge. (d) Behavior of subsequent *in situ* Na plating. (d) Potential profile during first cycle of plating and stripping of *in situ* Na plating at 0.5 mA cm^{-2} and 5.6 MPa. (e) Cycling at 0.2 mA cm^{-2} with a capacity of 2.0 mA h cm^{-2} and a stack pressure of 5.6 MPa and at room temperature. Copyright 2024, American Chemical Society.

concentration and hard short circuiting (Fig. 7c). Electrochemical impedance spectroscopy revealed a stable impedance response in the low-frequency region during sodium deposition, consistent with the formation of a uniform sodium electrode at the interface (Fig. 7d). This optimized interface enabled exceptional cycling reversibility, sustaining over 300 cycles at an areal capacity of 1 mA h cm^{-2} with an average coulombic efficiency exceeding 98% (Fig. 7e), highlighting excellent cycling reversibility. By elucidating the critical role of metal-ceramic interfacial contact in governing sodium nucleation and growth at solid–solid interfaces, this study provides key insights for advancing current collector in AFSSBs.

3.3 Interface modification: creating multifunctional artificial interphases

Direct modification of the electrolyte|current collector interface is a powerful tactic to lower nucleation barriers and guide uniform deposition. To tackle the dual issues of high nucleation overpotential and uneven Na^+ flux, Sun *et al.* proposed an interfacial regulation strategy based on the spontaneous polarization of ferroelectric $BaTiO_3$ that simultaneously mitigates uneven Na deposition and slow Na^+ replenishment.[37] Their approach involves fabricating a resilient ferroelectric composite substrate on an aluminum current collector. The ferroelectric substrate exhibits markedly enhanced interfacial sodium affinity and thereby reduces the nucleation overpotential for sodium deposition from 52.7 mV (on bare Al) to 4.3 mV (Fig. 8a and b). Through the generation of a built-in electric field, this substrate regulates the interfacial Na^+ distribution gradient, thereby promoting uniform and dense sodium deposition, while also functioning as a buffer layer to maintain interfacial intimacy (Fig. 8c). The performance of cells with this interface improves significantly. At the full-cell level, a cell with a $Na_3V_2(PO_4)_3$ cathode and $Na_3Zr_2Si_2PO_{12}$(NZSP) solid electrolyte shows good performance, with an initial coulombic efficiency of 94% and a capacity retention of 95.5% after 300 cycles (Fig. 8d and e). This work presents a novel strategy for developing high-energy-density and safe ceramic-electrolyte-based AFSSBs.

Our group recently used multiscale characterization to understand the degradation mechanism of anode-free solid-state batteries.[76] Specifically, it is revealed that at the Cu/NSSO interface, sodium forms either dendrites (good contact) or inert spherical aggregates (poor contact), both leading to dead sodium accumulation (Fig. 8f). Together with partial inactive encapsulated deposited sodium by a brittle SEI layer derived from interfacial side-reaction, the dead sodium leads to low coulombic efficiency. Based on this understanding, an iodinated polymeric elastic interphase (*I*-PIL) was designed. The *I*-PIL provides atomic-level bonding for uniform Na^+ flux while I_3^- species chemically reactivate dead sodium ($\Delta G = -5.46$ eV, Fig. 8g). This dual functionality enables Na||Cu half-cells to achieve 99.7% CE over 1000 h at 1.5 mA cm^{-2} (Fig. 8h and i). Full cells with $Na_3V_2(PO_4)_3$ cathodes retain 85.8% capacity after 2000 cycles at 1.0 mA cm^{-2} and 92.8% after three months under 28 mg cm^{-2} loading (Fig. 8j and k).

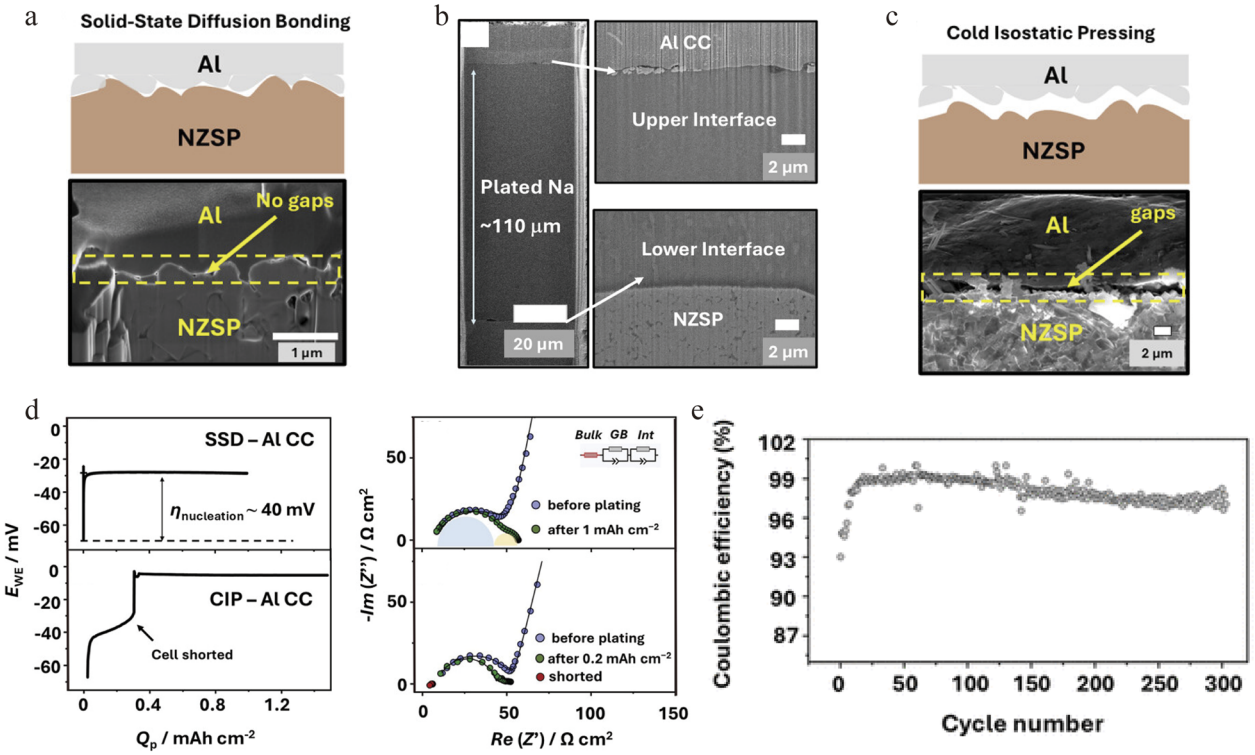

Fig. 7 Enabling uniform sodium deposition and reversible stripping toward anode free sodium solid state batteries at low stack pressure. Schematic illustration and FIB-SEM cross-section of the (a) solid-state diffusion (SSD) bonding method to achieve conformal contact and (c) cold isostatic press (CIP) method with a UV-ozone-treated aluminum CC showing gaps at the Al|NZSP interface. Morphology of electrodeposited sodium at the SSD bonded Al|NZSP interface. (b) FIB-SEM cross-sections at the center after high areal capacity plating of 12.5 mA h cm^{-2} (~110 μm) at J_{app} = 0.5 mA cm^{-2} (d) electrodeposition of sodium with SSD and CIP bonded aluminum cc in a half cell (Na|NZSP|Al). (e) Coulombic efficiency *vs.* cycle number. Copyright 2025, American Chemical Society.

3.4 Advanced characterization: illuminating the black box of deposition

In spite of the above progress, the development of AFSSBs is still fundamentally restricted by limited understanding towards sodium deposition kinetics on a bare current collector. The core challenge of an "anode-free" or "anode-less" configuration lies in realizing uniform and dense metallic sodium electrodeposition on the interface between the current collector and the solid electrolyte during the first charge. Janek's group comprehensively investigated several possible parameters determining the kinetics of this process at a Cu|NaSICON interface (NZSP, chemical formula $Na_{3.4}Zr_2Si_{2.4}P_{0.6}O_{12}$), revealing that the deposition current density is the primary factor determining uniformity.[77] A relatively uniform sodium layer was obtained at a current density of ≈1 mA cm^{-2}, whereas variations in stack pressure showed a less influence (Fig. 9a–e). Although no harmful dendrite penetration was observed, sodium deposition could induce local mechanical damage to the NZSP electrolyte near the interface (Fig. 9f). This work confirms the feasibility of the concept and highlights that optimizing current density and ensuring intimate initial contact are key strategies for achieving uniform sodium plating.

Building on this parametric understanding, Janek's group further elucidated the deposition mechanism by probing its evolving microstructure.[67] The work provided transformative insights by applying cryogenic electron backscatter diffraction (EBSD) to electrodeposited Li and Na on solid electrolytes (Fig. 10a). They discovered that deposition often produces large, columnar grains (>100 μm) with boundaries perpendicular to the substrate (Fig. 10b). More importantly, *in situ* EBSD revealed two critical dynamic processes: grain coarsening during plating, where larger grains consume smaller ones *via* boundary migration (Fig. 10c). After the first stripping step, a dark region appears adjacent to the initially well contacted Na|NZSP interface (Fig. 10d(A)). This dark contrast is attributed to pore formation, which reduces the local secondary electron yield, as further evidenced by darker areas in Fig. 10d. This work links deposition conditions to crystallographic structure, providing a foundation for designing high-performance AFSSB through microstructure control.

4. Summary and future perspectives

This review has systematically analyzed the current landscape, challenges, and emerging strategies for AFSSBs. The pursuit of this ultimate energy-dense configuration for sodium-based electrochemistry is a tough yet imperative endeavor. We have detailed how the interconnected challenges of solid electrolyte limitations, undefined current collector roles, unstable solid–solid interfaces, and intrinsically inhomogeneous sodium

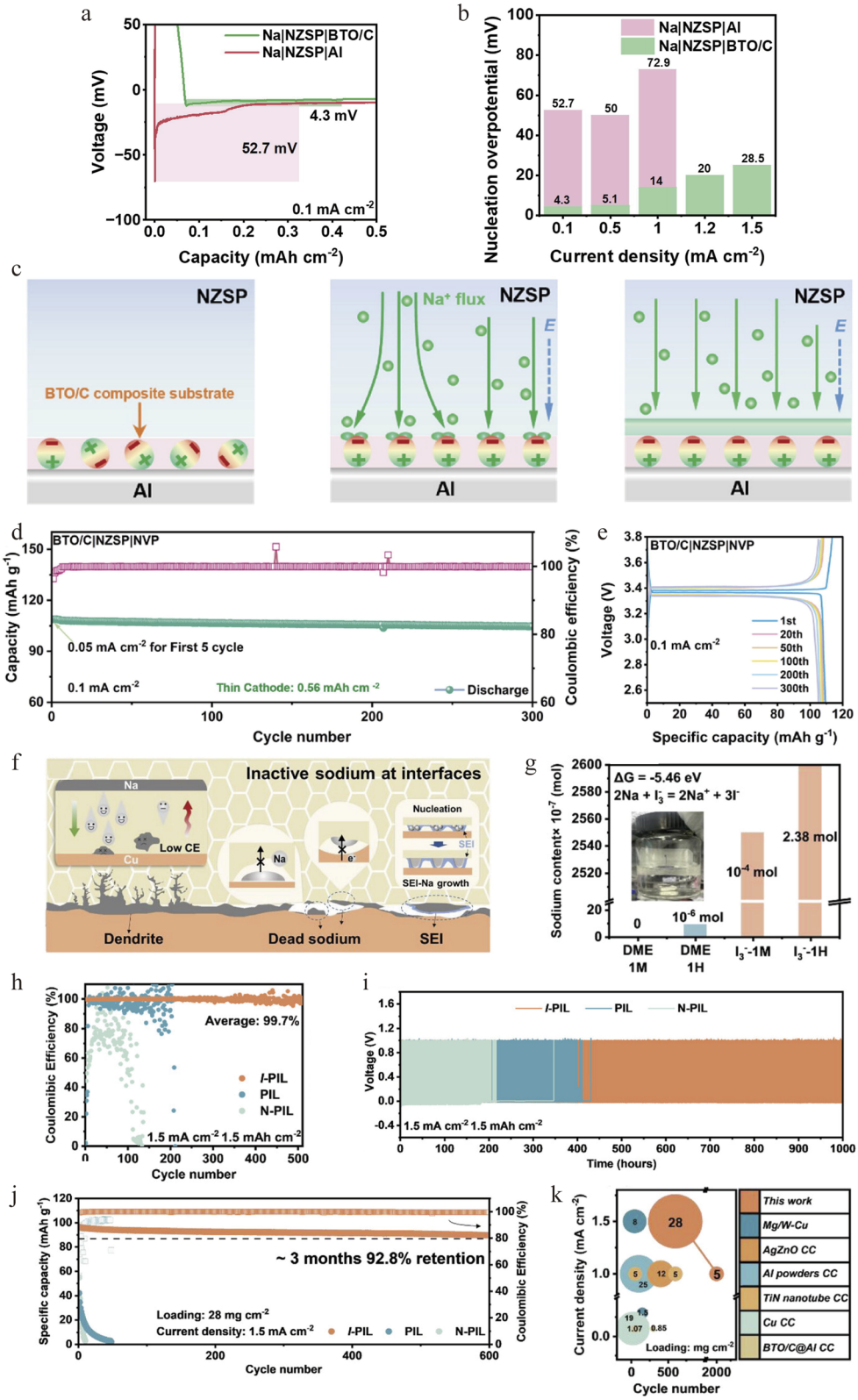

Fig. 8 Employing a ferroelectric interface to achieve efficient sodium metal cycling in anode-free solid-state batteries. (a) Galvanostatic discharge profile of Na|NZSP|BTO/C and Na|NZSP|Al at 0.1 mA cm^{-2}. (b) Nucleation potential of Na|NZSP|BTO/C and Na|NZSP|Al cells at various current densities. (c) Schematic illustration for the ferroelectric effect controlling sodium deposition. (d) Cycling performance and (e) selected charge–discharge profile of the BTO/C|NZSP|NVP cell at 0.1 mA cm^{-2} (test at current density of 0.5 mA cm^{-2}, at 1.3 MPa pressure). Copyright 2024, Elsevier B.V. *I*-PIL artificial interphase: synergistic dead sodium recovery and interfacial contact maintenance. (f) Schematic illustration of various dead sodium morphologies formed during cycling. (g) ICP-MS test results and Gibbs free energy calculation. (h) Coulombic efficiency and (i) galvanostatic cycling performance at current density of 1.5 mA cm^{-2} for 1.5 mA h cm^{-2}. (j) Cycling performance of AFSSB matched with high-load cathodes at a current density of 1.5 mA cm^{-2}. (k) Comparison of AFSSB cycling performance with other reported works, copyright 2026, Wiley-VCH GmbH.

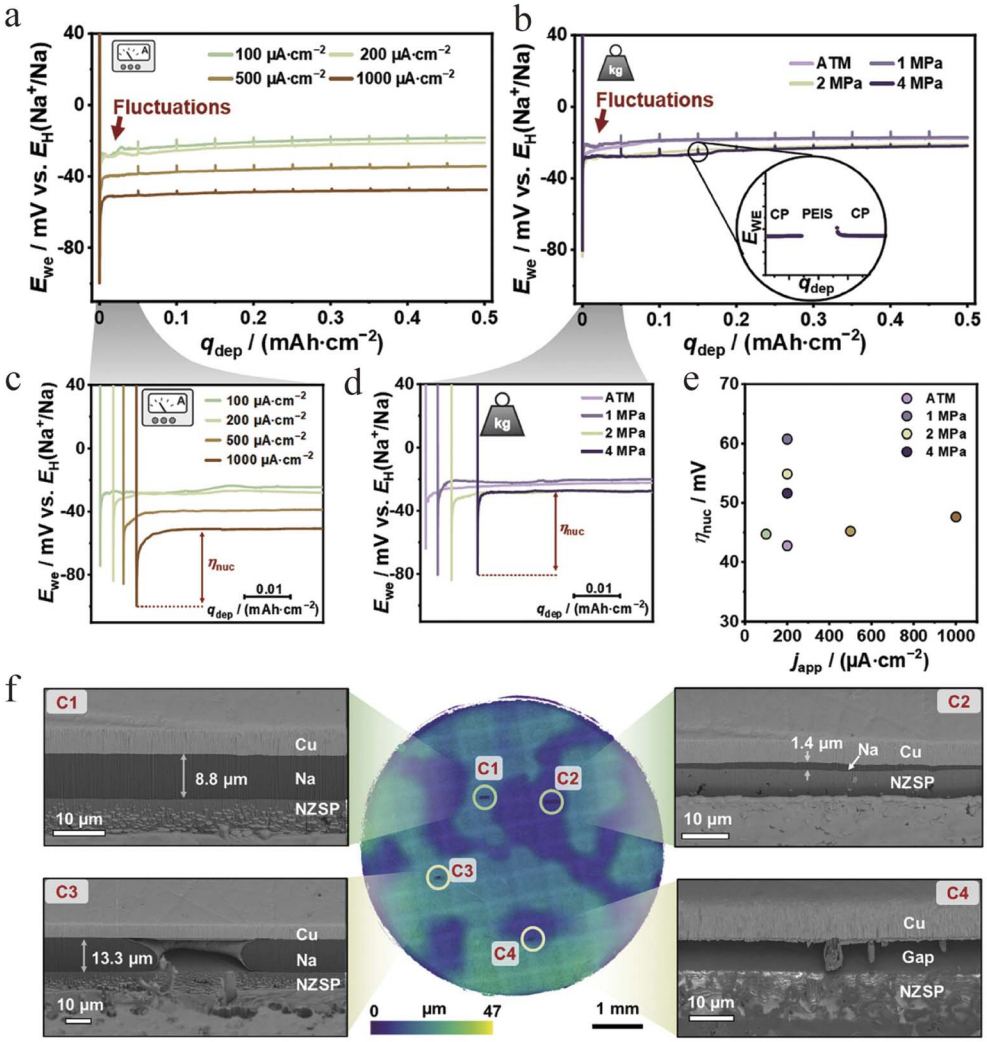

Fig. 9 Engineering sodium deposition at the copper–NaSICON interface for building reservoir-free solid-state sodium batteries. (a and b) potential profile of cathodic deposition of sodium at a Cu|NZSP interface at various (a) current densities and (b) stack pressures. A pressure of 2 MPa was applied for measurements at different current densities. The initial drop in the potential profile for both series is depicted at higher magnification for (c) current density and (d) stack pressure series to visualize the nucleation overpotential η_{nuc}. (e) The determined η_{nuc} for the current densities (green and brown points) and stack pressure series. (f) FIB-SEM cross-sections of selected spots on the copper electrode to visualize the sodium growth underneath. Copyright 2024, Wiley-VCH GmbH.

deposition collaboratively degrade performance. In response, innovative strategies are being developed across multiple fronts: hybrid electrolytes decouple transport from stability, engineered current collectors guide uniform nucleation, multifunctional interphases regulate ion flux, and advanced characterization reveals the critical microstructural dynamics of plating and stripping. These synergistic efforts are laying the groundwork for breaking the performance ceiling of AFSSBs. To drive AF-SSBs from promising prototypes to practical technologies, future research could pivot toward the following critical directions. Worth to note that, future efforts must not only push performance boundaries but also rigorously preserve the intrinsic cost advantage that motivates sodium-based chemistry in the first place, including material costs, processing expenses as well as cell-level manufacturing scalability.

(1) Current collectors beyond Cu and Al: exploring a new paradigm in current collector design. Future work could move beyond traditional Cu/Al foil-based current collectors to explore novel substrates with tailored functionalities. This includes investigating sodiophilic alloys, hierarchical scaffolds such as functionalized carbon that lower local current density. Composite current collectors integrating stress-buffering or ion-conducting phases could also be considered, yet the density of current collector must be taken in to consideration to align with the ultimate goal of AFSSBs, *i.e.*, the high energy density. The guiding principle should be to design collectors that reduces nucleation overpotential, spatially confining deposition, and mechanically accommodating volume changes rather than simply acting as a substrate.

(2) Deciphering solid-state-specific failure mechanisms. Unlike liquid systems, the failure modes in AFSSBs are

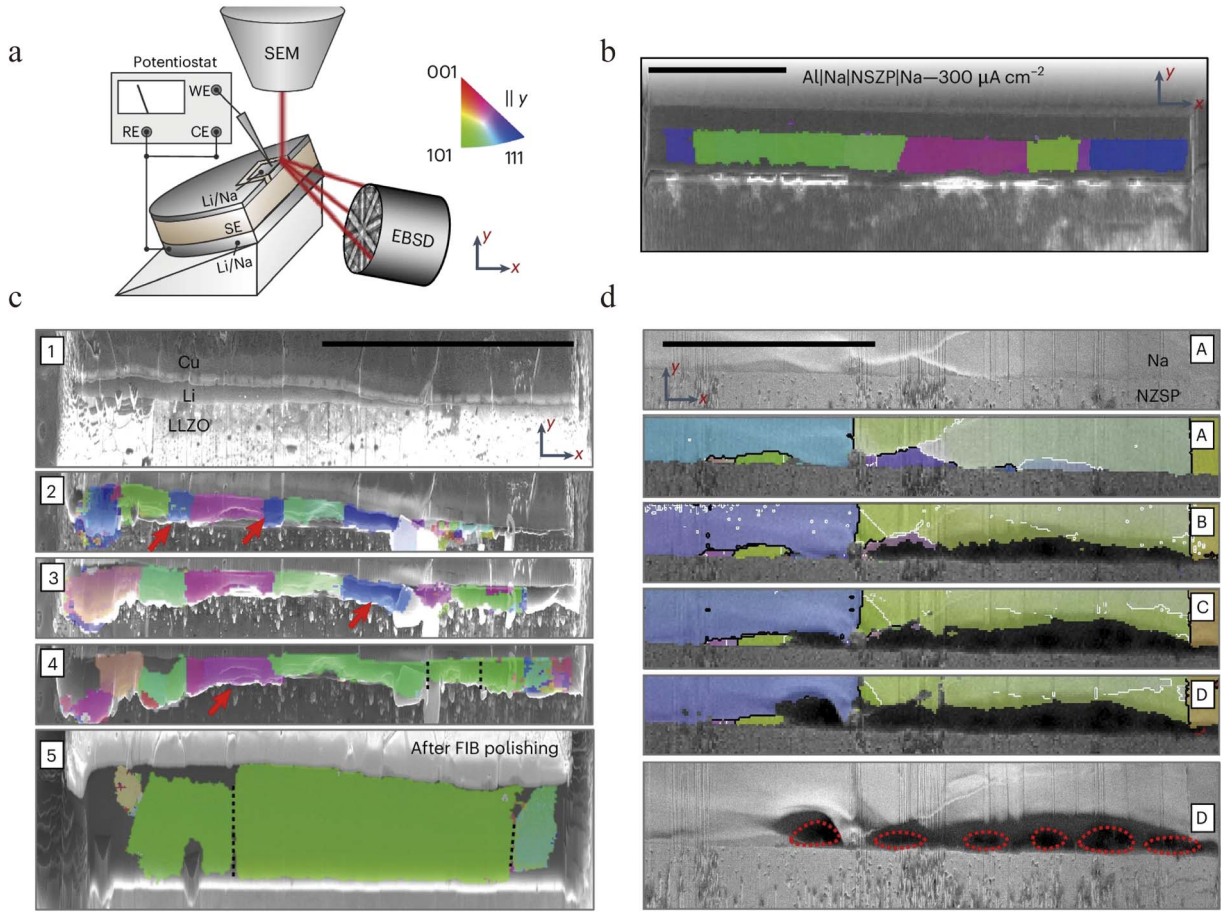

Fig. 10 (a) Schematic depiction of the *in situ* EBSD setup whereby RE, WE and CE denote the reference, working and counter electrode, respectively. (b) A cross-sectional IPF map of sodium plated at the Al|NZSP interface. (c and d) The microstructure evolution for lithium plating (c) and sodium stripping (d). The red arrows indicate grains disappearing during film growth in (c), and the red outlines indicate pores formed during stripping in d. The map provided in c step 5 was acquired after a 2 weeks storage period and second FIB polishing step. Scale bars, 100 μm. Copyright 2024, the Author(s).

governed by a complex interplay of electrochemistry and solid mechanics. A fundamental understanding of these unique mechanisms is urgently needed. Key questions include: How do the chemical composition, crystallinity, and mechanical properties (elastic modulus, fracture toughness) of different solid electrolytes (sulfides, oxides, borohydrides) dictate sodium filament growth modes? What is the precise role of stack pressure on sodium nucleation kinetics, stripping homogeneity, and void formation dynamics? How do the decomposition products of solid electrolytes form and evolve at the buried interface, and how do their mechanical properties impact contact loss? Clearly, these questions that are specific for solid-state electrolytes cannot be mirrored from liquid-based anode free cells, so as the corresponding solutions. Systematic studies combining *operando* techniques with mechanical modeling are essential to build predictive frameworks.

(3) Navigating the concept from "All-Solid" to "Practically-Solid". The binary choice between pure solid-state and liquid-electrolyte systems may be an unnecessary obsession. As long as the safety requirement can be fulfilled, a pragmatic development path is likely to involve a strategic gradient. In this context, quasi-solid-state systems (such as gel polymers, "liquid-in-solid" composites) offer an invaluable bridge, leveraging near-liquid satisfactory interfacial kinetics while significantly improving safety and suppressing dendrite growth. These systems can immediately address critical issues like interfacial resistance and CE. In parallel, fundamental research on strictly all-solid-state systems is also vital, in terms of focusing on ultra-stable interfaces (*e.g.*, through *in situ* formed protective layers) and understanding intrinsic ion transport and plating limits. The ultimate goal is to converge, where insights from quasi-solid systems inform the design of eventually solvent-free, high-performance all-solid-state batteries. The optimal solution may be application-dependent, balancing energy density, power, cycle life, safety, and cost.

In conclusion, the development of AFSSBs is a grand challenge that sits at the intersection of materials science, interfacial chemistry, and electro-mechanical engineering. Success will not come from a single breakthrough but from the concerted, cross-disciplinary integration of advances in electrolyte synthesis, interface engineering, and cell architecture design. By addressing the outlined perspectives, the scientific

community can transform the concept of anode-free solid-state sodium batteries into a cornerstone technology for the next generation of safe, high-energy-density, and resource-resilient energy storage.

Author contributions

Conceptualization: ZW and FD; writing – original draft: YZ and ZW; writing – review and editing: GS, HJ and FD.

Conflicts of interest

There are no conflicts to declare.

Data availability

No primary research results, software or code have been included and no new data were generated or analysed as part of this review.

Acknowledgements

This work was supported by the National Key R&D Program of China with Grant No. 2024YFE0209600 and National Natural Science Foundation of China with Grant No. 12274176 and 12574245. We also would like to thank the support from the Department of Science and Technology of Jilin Province with Grant No. 20240101310JC and the Fundamental Research Funds for the Central Universities, Jilin University.

References

1 J. Janek and W. G. Zeier, *Nat. Energy*, 2023, **8**, 230–240.
2 B. Luo, J. Wu, M. Zhang, Z. Zhang, X. Zhang, Z. Fang, Z. Xu and M. Wu, *Chem. Sci.*, 2023, **14**, 13067–13079.
3 B. Zhou, Y. Gao, X. Lin, B. Yang, N. Kang, Y. Qiao, H. Zhang, L. Li and S. Chou, *Chem. Sci.*, 2025, **16**, 13594–13628.
4 Z. Zhao, W. Ye, F. Zhang, Y. Pan, Z. Zhuo, F. Zou, X. Xu, X. Sang, W. Song and Y. Zhao, *Chem. Sci.*, 2023, **14**, 12219–12230.
5 X. Fan and C. Wang, *Chem. Soc. Rev.*, 2021, **50**, 10486–10566.
6 L. Wang, Z. Wang, Y. Bai, D. Yuan, J. Chen, S. X. Dou, H. K. Liu and C. Wu, *Adv. Mater.*, 2025, **37**, e10480.
7 Z. Hong, Z.-C. Jian, Y.-F. Zhu, Y.-J. Li, Q.-C. Ling, H. Xin, D. Wang, C. Wu and Y. Xiao, *Chem. Sci.*, 2025, **16**, 17058–17085.
8 Y. Liu, X. Hu, J. Li, G. Zhong, J. Yuan, H. Zhan, Y. Tang and Z. Wen, *Nat. Commun.*, 2022, **13**, 663.
9 Y. Huo, H. Guo, Z. Hong, L. Xie, Y. He, W. Cao, M. Xu, Y. Xiao and Y. Qi, *Angew. Chem.*, 2025, **137**, e202513023.
10 X. Wang, Z. Yang, Y. Cai, H. Ma, J. Xu, R. Khatoon, Z. Ye, D. Wang, M. T. Sajjad and J. Lu, *Nano-Micro Lett.*, 2026, **18**, 105.
11 G. Kothandam, G. Singh, X. Guan, J. M. Lee, K. Ramadass, S. Joseph, M. Benzigar, A. Karakoti, J. Yi and P. Kumar, *Advanced Science*, 2023, **10**, 2301045.
12 A. Alkhateeb and H. Ben Yahia, *ACS Omega*, 2020, **5**, 30799–30807.
13 M. Wan, R. Zeng, J. Meng, Z. Cheng, W. Chen, J. Peng, W. Zhang and Y. Huang, *Nano-Micro Lett.*, 2022, **14**, 9.
14 Q. Wang, C. Guo, Y. Zhu, J. He and H. Wang, *Nano-Micro Lett.*, 2018, **10**, 30.
15 N. Liu, X. Wang, J. Liu, N. Liu and L. Wang, *Chem. Sci.*, 2025, **16**, 14724–14732.
16 Q. Liu, Z. Hu, M. Chen, C. Zou, H. Jin, S. Wang, S. L. Chou, Y. Liu and S. X. Dou, *Adv. Funct. Mater.*, 2020, **30**, 1909530.
17 J. Peng, W. Zhang, Q. Liu, J. Wang, S. Chou, H. Liu and S. Dou, *Adv. Mater.*, 2022, **34**, 2108384.
18 Y. Dang, Z. Li, Y. Yu, X. Bai, L. Wang, X. Wang, P. Liu, C. Sun, X. Zhou, Z. Wang, *et al.*, *Research*, 2025, **8**, 0794.
19 W. Zuo, A. Innocenti, M. Zarrabeitia, D. Bresser, Y. Yang and S. Passerini, *Acc. Chem. Res.*, 2023, **56**, 284–296.
20 G. Gammaitoni, G. Cha, R. R. Kolan, S. Christiansen, F. Fauth and M. Bianchini, *EES Batteries*, 2025, **1**, 1596–1611.
21 C. Zhang, Y. Yang, X. Liu, M. Mao, K. Li, Q. Li, G. Zhang and C. Wang, *Innovation*, 2023, **4**, 100518.
22 H. Zhang, J. Li, J. Liu, Y. Gao, Y. Fan, X. Liu, C. Guo, H. Liu, X. Chen and X. Wu, *Nat. Commun.*, 2025, **16**, 2520.
23 Y. Singh, R. Parmar, S. Rani, M. Kumar, K. K. Maurya and V. N. Singh, *Heliyon*, 2022, **8**, e10013.
24 Elective, https://www.electrive.com/2023/02/23/hina-launches-sodium-ion-+battery-tests-in-vehicles/, accessed January, 2026.
25 B. Chen, J. Wang, Z. Xu, J. Miao, Y. Lu, Z. Yan, K. Zhang and J. Chen, *Adv. Mater.*, 2025, **37**, e09966.
26 X. Liu, J. Wang, M. Du, K. Robeyns, Y. Filinchuk, Q. Zhu, V. Kumar, Y. Garcia, G. Borodi and C. Morari, *Advanced Science*, 2022, **9**, 2200924.
27 A. Mauger and C. M. Julien, *Materials*, 2020, **13**, 3453.
28 X. Lu, S. Li, Y. Li, F. Wu, C. Wu and Y. Bai, *Adv. Mater.*, 2024, **36**, 2407359.
29 W. Liu, W. Cui, C. Yi, J. Xia, J. Shang, W. Hu, Z. Wang, X. Sang, Y. Li and J. Liu, *Nat. Commun.*, 2024, **15**, 9889.
30 Y. Gao, Z. Hou, M. Jiang, D. Lei, X. Zhang, Y. Zhang and J.-G. Wang, *J. Electroanal. Chem.*, 2023, **941**, 117525.
31 Z. Yang, J. Zhang, M. C. Kintner-Meyer, X. Lu, D. Choi, J. P. Lemmon and J. Liu, *Chem. Rev.*, 2011, **111**, 3577–3613.
32 Y. Cuiyun and Y. Chenghao, *Chem. J. Chinese Universities*, 2023, **44**, 20220728.
33 WND, https://subsites.chinadaily.com.cn/bizwnden/2024-06/03/c_992553.htm, accessed January, 2026.
34 Y.-B. Wu, H.-Y. Hu, J.-Y. Li, H.-H. Dong, Y.-F. Zhu, S.-Q. Chen, N.-N. Wang, J.-Z. Wang and Y. Xiao, *Chem. Sci.*, 2025, **16**, 3928–3937.
35 S.-Y. Li, Y.-L. Heng, Z.-Y. Gu, X.-T. Wang, Y. Liu, X.-R. Zhang, Z.-H. Sun, D.-H. Liu, B. Li and X.-L. Wu, *Chem. Sci.*, 2026, **17**(1), 137–150.
36 T. Yang, D. Luo, Y. Liu, A. Yu and Z. Chen, *iScience*, 2023, **26**, 105982.
37 C. Sun, Y. Li, Z. Sun, X. Yuan, H. Jin and Y. Zhao, *Mater. Today*, 2024, **80**, 395–405.

38 E. Kazyak, M. J. Wang, K. Lee, S. Yadavalli, A. J. Sanchez, M. Thouless, J. Sakamoto and N. P. Dasgupta, *Matter*, 2022, **5**, 3912–3934.
39 C. Haslam and J. Sakamoto, *J. Electrochem. Soc.*, 2023, **170**, 040524.
40 S. E. Sandoval, J. A. Lewis, B. S. Vishnugopi, D. L. Nelson, M. M. Schneider, F. J. Q. Cortes, C. M. Matthews, J. Watt, M. Tian and P. Shevchenko, *Joule*, 2023, **7**, 2054–2073.
41 W. Liu, Y. Luo, Y. Hu, Z. Chen, Q. Wang, Y. Chen, N. Iqbal and D. Mitlin, *Adv. Energy Mater.*, 2024, **14**, 2302261.
42 Y. An, Z. Pei, D. Luan and X. W. Lou, *Sci. Adv.*, 2025, **11**, eadx7124.
43 G. Deysher, J. A. S. Oh, Y.-T. Chen, B. Sayahpour, S.-Y. Ham, D. Cheng, P. Ridley, A. Cronk, S. W.-H. Lin, K. Qian, L. H. B. Nguyen, J. Jang and Y. S. Meng, *Nat. Energy*, 2024, **9**, 1161–1172.
44 P. Albertus, S. Babinec, S. Litzelman and A. Newman, *Nat. Energy*, 2018, **3**, 16–21.
45 J. Ruan, J. Hu, Q. Li, S. Luo, J. Yang, Y. Liu, Y. Song, S. Zheng, D. Sun and F. Fang, *Nat Sustainability*, 2025, 1–12.
46 T. Deng, X. Ji, L. Zou, O. Chiekezi, L. Cao, X. Fan, T. R. Adebisi, H.-J. Chang, H. Wang and B. Li, *Nat. Nanotechnol.*, 2022, **17**, 269–277.
47 Y. Su, X. Rong, A. Gao, Y. Liu, J. Li, M. Mao, X. Qi, G. Chai, Q. Zhang and L. Suo, *Nat. Commun.*, 2022, **13**, 4181.
48 M. D. Slater, D. Kim, E. Lee and C. S. Johnson, *Adv. Funct. Mater.*, 2013, **23**, 947–958.
49 T. Yu, C. Zeng, H. Cheng, D. Luo, B. Liu, G. Liu and Z. Lu, *Adv. Sustainable Syst.*, 2025, **9**, e00687.
50 H. Lin, D. Patrun, G. Pandey, F. Dong, T. J. K. Schneider, J. Tao, Y. Lin and S. Mathur, *Mater. Today Energy*, 2026, 102217.
51 E. Goikolea, V. Palomares, S. Wang, I. R. de Larramendi, X. Guo, G. Wang and T. Rojo, *Adv. Energy Mater.*, 2020, **10**, 2002055.
52 K. Abraham, *ACS Energy Lett.*, 2020, **5**, 3544–3547.
53 F. Zhongheng, C. Xiang, Y. Nan, Y. Legeng, S. Xin, Z. Rui and Z. Qiang, *Chem. J. Chinese Universities*, 2023, **44**, 20220703.
54 J. Schuett, J. Schillings and S. Neitzel-Grieshammer, *Phys. Chem. Chem. Phys.*, 2024, **26**, 2190–2204.
55 L. X. Zhang, Y. M. Liu, Y. You, A. Vinu and L. Q. Mai, *Interdiscip. Mater.*, 2023, **2**(1), 91–110.
56 K. B. Hatzell, X. C. Chen, C. L. Cobb, N. P. Dasgupta, M. B. Dixit, L. E. Marbella, M. T. McDowell, P. P. Mukherjee, A. Verma and V. Viswanathan, *ACS Energy Lett.*, 2020, **5**, 922–934.
57 Z. Xu, C. Lin, J. Qiu and Z. Wang, *Adv. Mater.*, 2025, 2506037.
58 Y. Wang, Y. Wang, Y.-X. Wang, X. Feng, W. Chen, X. Ai, H. Yang and Y. Cao, *Chem*, 2019, **5**, 2547–2570.
59 J. A. Lewis, K. A. Cavallaro, Y. Liu and M. T. McDowell, *Joule*, 2022, **6**, 1418–1430.
60 S. Tang, Z. Qiu, X.-Y. Wang, Y. Gu, X.-G. Zhang, W.-W. Wang, J.-W. Yan, M.-S. Zheng, Q.-F. Dong and B.-W. Mao, *Nano Energy*, 2018, **48**, 101–106.
61 K.-T. Tseng, K. Lee and J. Sakamoto, *ACS Energy Lett.*, 2024, **9**, 4544–4549.
62 M. Wang, J. Yang, H. Ji, Z. Li, F. Wang, F. Fang, J. Ruan, D. Sun and F. Wang, *Nat. Commun.*, 2025, **17**, 264.
63 M. Geng, D. Han, Z. Huang, S. Wang, M. Xiao, S. Zhang, L. Sun, S. Huang and Y. Meng, *Energy Storage Mater.*, 2022, **52**, 230–237.
64 O. J. Dahunsi, S. Gao, J. Kaelin, B. Li, I. B. A. Razak, B. An and Y. Cheng, *Nanoscale*, 2023, **15**, 3255–3262.
65 R. Li, D. C. Jiang, P. Du, C. B. Yuan, X. Y. Cui, Q. C. Tang, J. Zheng, Y. C. Li, K. Lu, X. D. Ren, *et al.*, *Chem. Sci.*, 2022, **13**(47), 14132–14140.
66 J. Chen, Q. Li, T. P. Pollard, X. Fan, O. Borodin and C. Wang, *Mater. Today*, 2020, **39**, 118–126.
67 T. Fuchs, T. Ortmann, J. Becker, C. G. Haslam, M. Ziegler, V. K. Singh, M. Rohnke, B. Mogwitz, K. Peppler, L. F. Nazar, J. Sakamoto and J. Janek, *Nat. Mater.*, 2024, **23**, 1678–1685.
68 S. E. Sandoval and M. T. McDowell, *Matter*, 2023, **6**, 2101–2102.
69 D. K. Singh, T. Fuchs, C. Krempaszky, P. Schweitzer, C. Lerch, F. H. Richter and J. Janek, *Matter*, 2023, **6**, 1463–1483.
70 D. K. Singh, T. Fuchs, C. Krempaszky, B. Mogwitz, S. Burkhardt, F. H. Richter and J. Janek, *Adv. Funct. Mater.*, 2023, **33**, 2211067.
71 M. K. Tufail, P. B. Zhai, W. Khokar, M. Y. Jia, N. Zhao and X. X. Guo, *Interdiscip. Mater.*, 2023, **2**(4), 529–568.
72 Z. Lu, H. Yang, G. Wu, P. Shan, H. Lin, P. He, J. Zhao, Y. Yang and H. Zhou, *Adv. Mater.*, 2024, **36**, 2404569.
73 Y. Kim, M. Künzel, D. Steinle, X. Dong, G.-T. Kim, A. Varzi and S. Passerini, *Energy Environ. Sci.*, 2022, **15**, 2610–2618.
74 W. Feng, C. Li, P. Wang, J. Hu, X. Yu, Y. Zhang, X. Zhu, D. Zhang, Y. Xia and Y. Zhao, *Chem. Eng. J.*, 2025, **512**, 162467.
75 V. K. Singh, J. Schuler, T. Ortmann, M. Ziegler, J. r. Janek and L. F. Nazar, *ACS Energy Lett.*, 2025, **10**, 3663–3669.
76 B. Yi, Y. Xia, H. Jiang, N. Chen, J. Sun, Z. Wei and F. Du, *Adv. Mater.*, 2026, **38**, e20758.
77 T. Ortmann, T. Fuchs, J. K. Eckhardt, Z. Ding, Q. Ma, F. Tietz, C. Kübel, M. Rohnke and J. Janek, *Adv. Energy Mater.*, 2024, **14**, 2302729.